GeroScience
https://doi.org/10.1007/s11357-026-02314-8

ORIGINAL ARTICLE

Galectin-3 binding protein is upregulated in heart failure with preserved ejection fraction and associated with endothelial nitric oxide synthase deficiency

Rosalinda Madonna · Maria Concetta Cufaro · Samuele Gagliardi · Riccardo Morganti · Fabio Di Ferdinando · Sandra Ghelardoni · Alessandra Marzoppi · Ashot Avagimyan · Vincenzo Lionetti · Giuseppe Ambrosio · Francesco Fedele · Piero Del Boccio

Received: 18 March 2026 / Accepted: 5 May 2026
© The Author(s), under exclusive licence to American Aging Association 2026

Abstract Heart failure with preserved ejection fraction (HFpEF) is a cardiometabolic syndrome strongly associated with aging, systemic inflammation and endothelial dysfunction, in which impaired endothelial nitric oxide synthase (eNOS) signaling plays a central role. This study aimed to identify circulating proteins associated with HFpEF and to explore their relationship with endothelial alterations under metabolic stress. A total of 109 HFpEF patients and 49 control subjects underwent clinical, laboratory, and echocardiographic assessment. HFpEF patients exhibited a high burden of cardiometabolic comorbidities and significantly increased NT-proBNP (2851.2 ± 1565.5 vs 156.0 ± 85.2 pg/mL) and C-reactive protein levels (2.9 ± 4.5 vs 0.31 ± 0.33 mg/dL). Echocardiography revealed elevated filling pressures (E/e′ 16.5 ± 3.8 vs 7.0 ± 1.9), a higher prevalence of high-probability pulmonary hypertension, and impaired right ventricular–pulmonary artery coupling. Exploratory proteomic profiling identified galectin-3 binding protein (LGALS3BP)

Supplementary Information The online version contains supplementary material available at https://doi.org/10.1007/s11357-026-02314-8.

R. Madonna (✉) · S. Gagliardi · G. Ambrosio · F. Fedele
Department of Surgical, Medical and Molecular Pathology and Critical Area, University of Pisa, Pisa, Italy
e-mail: rosalinda.madonna@unipi.it

R. Madonna
Cardiology Division, Pisa University Hospital, Via Paradisa, 2, 56124 Pisa, Italy

M. C. Cufaro · F. Di Ferdinando
Department of Innovative Technologies in Medicine & Dentistry, 'G. d'Annunzio' University University of Chieti Pescara, Chieti, Italy

M. C. Cufaro · F. Di Ferdinando · P. Del Boccio (✉)
Center for Advanced Studies and Technology (CAST), G. d'Annunzio' University of Chieti Pescara, Chieti, Italy
e-mail: piero.delboccio@unich.it

R. Morganti
Statistical Support to Clinical Trials Department, University of Pisa, 56126 Pisa, Italy

S. Ghelardoni
Department of Surgical, Medical and Molecular Pathology and Critical Area, Laboratory of Biochemistry, University of Pisa, Pisa, Italy

A. Marzoppi
National Institute for Cardiovascular Research (INRC), Bologna, Italy

A. Avagimyan
Yerevan State Medical University After M. Heratsi, Yerevan, Armenia

V. Lionetti
Unit of Translational Critical Care Medicine, Laboratory of Basic and Applied Medical Sciences, Interdisciplinary Research Center "Health Science," Scuola Superiore Sant'Anna, Pisa, Italy

G. Ambrosio
Cardiology Department, Santa Maria Della Misericordia Hospital, Perugia, Italy

Published online: 11 May 2026

as increased in plasma from HFpEF patients, a finding confirmed by ELISA showing significantly higher circulating levels compared with controls (8.65 ± 0.66 vs 2.36 ± 0.26 ng/mL, $p < 0.001$). Pathway analysis suggested a potential association between LGALS3BP and activation of nitric oxide synthase 2 *(NOS2)*-related inflammatory pathways. In vitro, metabolic stress conditions increased LGALS3BP expression in murine endothelial cells, with a more pronounced response in $eNOS^{-/-}$ cells. In addition, eNOS deficiency was associated with the appearance of a lower-molecular weight LGALS3BP form and with increased markers of endothelial senescence and autophagy. LGALS3BP is elevated in HFpEF and is associated with endothelial alterations linked to impaired eNOS signaling under metabolic stress. These findings suggest a potential connection between endothelial stress responses and LGALS3BP expression in HFpEF, supporting further investigation of this protein as a biomarker of endothelial dysfunction in age-related cardiometabolic disease.

Keywords Heart failure with preserved ejection fraction (HFpEF) · LGALS3BP · Endothelial dysfunction · Endothelial nitric oxide synthase (eNOS) · Inflammation · Endothelial stress · Biomarkers

Introduction

Heart failure (HF) is a complex clinical syndrome characterized by structural and functional alterations of cardiac performance that impair the ability of the heart to maintain adequate tissue perfusion without elevated filling pressures. Clinically, HF manifests with symptoms and signs such as dyspnea, fatigue, and peripheral edema [1]. HF is commonly classified according to left ventricular ejection fraction (LVEF), a parameter used for clinical characterization and therapeutic stratification. Based on LVEF, HF is categorized as heart failure with reduced ejection fraction (HFrEF, LVEF ≤ 40%), mildly reduced ejection fraction (HFmrEF, LVEF 41–49%), and preserved ejection fraction (HFpEF, LVEF ≥ 50%) [2]. Among these phenotypes, HFpEF represents a clinically and biologically distinct form of HF characterized by symptoms and signs of HF despite preserved systolic function. HFpEF is increasingly recognized as a cardiometabolic and age-associated syndrome. Its prevalence rises markedly with aging [3] and it frequently coexists with systemic comorbidities such as arterial hypertension, diabetes mellitus, obesity, and metabolic syndrome [4]. These conditions contribute to the development of chronic low-grade inflammation and widespread vascular dysfunction that are thought to play a major role in HFpEF pathophysiology [4, 5]. In this context, endothelial and microvascular dysfunction have emerged as key mechanisms contributing to impaired cardiac relaxation, increased myocardial stiffness, and abnormal ventricular–vascular coupling [6].Under physiological conditions, the endothelium regulates vascular tone, blood flow, and tissue homeostasis, largely through nitric oxide (NO) production, which is generated by endothelial nitric oxide synthase (eNOS) [7]. In HFpEF, chronic exposure to metabolic and inflammatory stress is associated with endothelial dysfunction and reduced NO bioavailability, leading to microvascular impairment and altered myocardial relaxation. Beyond its role in vascular tone regulation, the endothelium contributes to myocardial homeostasis through paracrine signaling that modulates cardiomyocyte growth, extracellular matrix turnover, and coronary perfusion. Disruption of this endothelial–myocardial cross-talk has been proposed as a contributor to myocardial hypertrophy, fibrosis, and increased ventricular stiffness observed in HFpEF. Chronic inflammatory states and aging-related vascular stress may further exacerbate endothelial alterations by promoting the release of pro-inflammatory mediators and adhesion molecules such as VCAM-1 [8], both established markers of endothelial dysfunction and microvascular injury. In parallel, reduced NO signaling together with increased oxidative stress and vasoconstrictor signaling (i.e.: endothelin-1, angiotensin II) have been associated with endothelial senescence and altered autophagic responses [9–11], processes that

F. Fedele
Department of Clinical, Internal, Anesthesiology and Cardiovascular Sciences, Sapienza University of Rome, Viale del Policlinico, 155, 00161 Rome, Italy

P. Del Boccio
Department of Science, 'G. d'Annunzio' University of Chieti-Pescara, Chieti, Italy

may contribute to vascular dysfunction and myocardial remodeling [8, 12–14]. Despite the growing recognition of endothelial dysfunction and impaired eNOS signaling in HFpEF, the molecular pathways linking eNOS alterations to inflammatory and stress-response mechanisms remain incompletely understood.

To explore these mechanisms, we performed proteomic analyses of samples from HFpEF patients to identify circulating proteins associated with this condition. Among the proteins identified, galectin-3 binding protein (LGALS3BP) emerged as a candidate molecule of interest. Importantly, the present study was designed to specifically investigate LGALS3BP as a mechanistic link between metabolic stress, eNOS dysfunction, and vascular inflammation in HFpEF, thereby providing a conceptual advance beyond its previously described role as a circulating inflammatory marker.

LGALS3BP is encoded by a gene located on human chromosome 17, producing a secreted multifunctional glycoprotein involved in extracellular matrix interactions, cell adhesion, and modulation of the low-grade inflammatory responses [15], suggesting a potential link with vascular and inflammatory alterations observed in HFpEF. Indeed, LGALS3BP modulates the bioavailability and signaling of multiple galectins, particularly galectin-3, a molecule consistently implicated in myocardial fibrosis, diastolic dysfunction, and adverse outcomes in HFpEF [16].

To further investigate the relationship between LGALS3BP expression and endothelial stress responses, we employed an in vitro model of murine aortic endothelial cells derived from wild-type and eNOS knock-out mice. This reductionist model was used to reproduce selected aspects of endothelial dysfunction under metabolic stress conditions. Although it does not fully recapitulate the complexity of HFpEF in vivo, it is an invaluable experimental system to study vascular biology and nitric oxide–dependent endothelial stress pathways [17]. However, it does not capture systemic contributors to HFpEF, including immune activation, neurohormonal signaling, and hemodynamic loading conditions, which are acknowledged limitations. Using this integrated clinical and experimental approach, we aimed to explore the association between LGALS3BP expression, endothelial dysfunction, and metabolic stress, thereby providing insights into molecular pathways potentially involved in HFpEF pathophysiology.

Materials and methods

Patient enrollment

This prospective, single-center, observational clinical study enrolled patients with a diagnosis of HFpEF at the Cardiology Division of the University Hospital of Cisanello, Pisa University, in Pisa (Italy). The study was conducted in accordance with the Helsinki Declaration. All procedures were approved by the local Institutional Ethics Committee for Human Studies (Protocol code PH-HF released by CEAVNO). All patients provided informed consent before each diagnostic test, which was carried out exclusively for clinical purposes. Local investigators had full access to patient data and medical records. Enrolment occurred between January 2022 and September 2023, with a total of 109 HFpEF patients and 50 healthy controls matched for sex, age and BMI included in the study. Human plasma samples from patients diagnosed with HFpEF and control subjects were used for proteomic analysis. The diagnosis of HFpEF was made following the criteria recommended by the current guidelines on HF of the Heart Failure Association of the European Society of Cardiology [18]. Moreover, a H2FPEF score > 6 was required [19], as well as no evidence of specific cardiac disease presenting with HFpEF (e.g., cardiac amyloidosis), significant coronary artery disease (> 70% stenosis of at least 1 epicardial coronary artery), and no history of acute coronary syndrome within the last 6 months. The following were additional exclusion criteria: pregnancy and breastfeeding, cancer or any other life-threating condition, Glomerular Filtration Rate < 30 ml/min/1.73 m^2, use of continuous parenteral inotropic agents, systolic BP < 90 mm Hg, narcotic abuse and/or excessive alcohol, psychiatric disease incompatible with being in study or any other medical or physical condition precluding the subject's participation.

Mono and 2D Transthoracic Echocardiography

Transthoracic echocardiography was performed by independent experienced cardiologists using a Philips iE33 echocardiograph (Philips xMATRIX

echocardiography system, Andover, MA, USA), according to the protocol reported in Online supplement.

Proteomics analyses

Proteomic analysis was performed as an exploratory discovery approach to identify candidate circulating proteins associated with HFpEF. Proteomic profiling was conducted using a comparative shotgun proteomics approach on two pooled plasma samples obtained from HFpEF patients and controls (n = 23 per group). Protein concentration was determined using the Bradford assay (Bio-Rad, Hercules, CA, USA) using bovine serum albumin (BSA, Sigma-Aldrich, St. Louis, MI, USA) as a calibration standard. A total of 40 µg of protein from each pool was subjected to enzymatic digestion using the SP3 protocol [20] with trypsin (Sigma-Aldrich). For label-free protein identification and quantification, peptides were analyzed in technical triplicate by LC–MS/MS using the UltiMate™ 3000 UPLC system (Thermo Fisher Scientific, Waltham, MA, USA) coupled to the Orbitrap Fusion™ Tribrid™ mass spectrometer (Thermo Fisher Scientific). Samples were first loaded onto a C18 Trap cartridge (0.3 mm ID, 5 mm L, 5 µm PS, Thermo Fisher Scientific) and then separated on an EASY-spray Acclaim™ PepMap™ C18 column (75 µm ID, 25 cm L, 2 µm PS, Thermo Fisher Scientific), using chromatographic conditions previously described [21] with a gradient length of 65 min. Mass spectrometry proteomics data have been deposited to the ProteomeXchange Consortium via the PRIDE partner repository with the dataset identifier Project accession**:** PXD075688, Token**:** oOTnWYyIz3dD. Raw proteomic data were processed with MaxQuant software (version 1.6.10.50; Max-Planck Institute for Biochemistry, Martinsried, Germany). The Andromeda search engine was used for peptide identification against the UniProt database (released 2025_02, taxonomy Homo Sapiens, 83,607 entries). Data processing parameters were set as previously described by us [22]. Briefly, carbamidomethylation of cysteine (C) residues was set as fixed modification, while oxidation of methionine (M) and deamidation of asparagine (N) and glutamine (Q) were defined as variable modifications. The false discovery rate (FDR) was set to 1% for both protein and peptide levels, as previously defined by us [21, 22]. Label-free quantification (LFQ intensity) was used to estimate relative protein abundance [23]. Differential protein expression between HFpEF and control groups was assessed using univariate statistical analysis with a significance threshold of $p < 0.05$, and results were visualized using volcano plot representation,. Identified protein ratios were subsequently analyzed using Ingenuity Pathway Analysis (IPA; Qiagen, Hilden, Germany) to perform Gene Ontology and functional enrichment analyses, as previously described [20]. Briefly, IPA enables prediction of activation (z-score ≥ 2.0) or inhibition (z-score ≤ -2.0) of upstream regulators and biological pathways based on curated literature knowledge [24].

Enzyme-Linked Immunosorbent Assay

For validation analyses, circulating LGALS3BP levels were measured in individual plasma samples from HFpEF patients and control subjects using a commercially available enzyme-linked immunosorbent assay (ELISA) kit for human galectin-3 binding protein (LGALS3BP; HUEB1734). Assays were performed according to the manufacturer's instructions. Plasma samples were analyzed in duplicate, and absorbance was measured using a microplate reader at the recommended wavelength. LGALS3BP concentrations were calculated from a standard curve generated using recombinant standards provided with the kit and are reported as ng/mL.

Blood chemistry analyses

Venous blood samples were drawn at hospital admission and plasma fractions were separated and stored in aliquots at − 80 °C until usage for omics analyses and enzyme-linked immunosorbent assay (ELISA) measurement of galectin-3 binding protein. Validation experiments using human galectin-3-binding protein (LGALS3BP) ELISA Kit (HUEB1734), were performed in all samples. Detailed procedures are reported in the Online supplement.

Cell culture and experimental model

Mouse aortic endothelial cells (MAECs) were obtained from Creative Bioarray (C57BL/6 MAECs, CSC-C1861; eNOS knockout MAECs, CSC-C8540W). WT MAECs were cultured in SuperCult®

C57BL/6 Mouse Aortic Endothelial Cell Medium (CM-C1861) and eNOS KO MAECs in SuperCult® eNOS KO Mouse Aortic Endothelial Cell Medium (CM-8540W), following the manufacturer's instructions. Both media contained basal glucose (5.5 mM) and were supplemented with 10% fetal bovine serum (FBS). Cells were maintained at 37 °C in a humidified incubator with 5% CO_2. Experiments were performed using cells at passage 4, and treatments were initiated when cultures reached approximately 70% confluence.

Metabolic treatments

Wild type (WT) and eNOS knock-out (KO) MAECs cells were exposed to different metabolic conditions for 24 h. Cells were treated with normal glucose (5.5 mM), high glucose (HG, 30 mM) [25], high insulin (HI, 10 nM) [26], and combination of high glucose and high insulin (HG + HI) [27]. At the end of the treatment period, cells were collected for protein extraction and functional assays as described below.

Protein extraction and Western blot analysis

Total cellular proteins were extracted using RIPA lysis buffer supplemented with protease and phosphatase inhibitors. Protein concentrations were determined prior to electrophoresis to ensure equal protein loading. Equal amounts of protein (30 µg per lane) were loaded for each condition and separated by SDS-PAGE and transferred onto PVDF membranes. Membranes were blocked with 3% bovine serum albumin (BSA) and incubated overnight at 4 °C with primary antibodies diluted in 3% BSA against AKT (1:1000), phospho-AKT (1:1000), ERK1/2 (1:1000), phospho-ERK1/2 (1:1000) (Cell Signaling technology, USA), endothelial nitric oxide synthase (1:500, eNOS, Santa Cruz Biotechnology, USA) and pENOS (1:500, Santa Cruz Biotechnology, USA), vascular cell adhesion molecule-1 (1:200, VCAM-1 Merck KGaA, Darmstadt, Germany), and Galectin-3 binding protein (LGALS3BP) (1:200, Santa Cruz Biotechnology). β-actin (1:5000) was used as a loading control. Membranes were then incubated with appropriate secondary antibodies diluted in 3% BSA for 1 h at room temperature. Immunoreactive bands were detected by chemiluminescence. Densitometric analysis was performed using ImageLab (Biorad) software and protein expression levels were normalized to β-actin. All experiments were performed in technical triplicate.

Autophagy assay

Autophagic activity was assessed using the Autophagy Assay Kit (ab139484, Abcam), according to the manufacturer's instructions. WT and eNOS KO MAECs subjected to the different metabolic treatments were incubated with the autophagy detection reagent to evaluate autophagosome formation. Autophagy levels were quantified following the kit protocol and expressed as the percentage of autophagy-positive cells [28].

Senescence-associated β-galactosidase staining

Cellular senescence was assessed using a Cellular Senescence Assay Kit (Merck KGaA, Darmstadt, Germany), according to the manufacturer's instructions. After metabolic treatments, cells were fixed and stained to detect senescence-associated β-galactosidase (SA-β-gal) activity, the gold standard hallmark of senescent endothelial cells [29]. Senescent cells were identified by blue cytoplasmic staining and quantified by manual counting. Results were expressed as the percentage of SA-β-gal–positive cells relative to the total number of cells.

PNGase F deglycosylation assay

To investigate the glycosylation status and processing of LGALS3BP, a PNGase F digestion assay was performed using the PNGase F Glycan Cleavage Kit (Gibco™), according to the manufacturer's instructions. Briefly, 25 µg of total protein from WT and eNOS KO MAECs were subjected to denaturing conditions prior to PNGase F treatment [30]. Following enzymatic digestion, samples were analyzed by Western blot using an anti-LGALS3BP antibody to assess changes in protein molecular weight.

Statistical analysis

Results are expressed as the mean ± SD. Differences among groups in metabolic treatments were analyzed by one-way ANOVA. In the experiments aimed at determining differences among groups, Tukey's

multiple comparison test was applied. To compare group variable with continuous and categorical variables in clinical profile and comorbidities, t-test for independent samples and chi square test were applied, respectively. A p value < 0.05 was considered statistically significant and analyses were performed by SPSS technology (v.30) and GraphPad Prism version 6.0 for Windows (GraphPad Software, San Diego, CA, USA). All in vitro experiments were independently repeated at least three times, and densitometric quantifications represent the mean of independent biological replicates.

Results

Clinical profile and comorbidities

A clear clinical distinction was observed between the control population ($n = 49$) and the HFpEF group ($n = 109$). Patients were significantly older than controls (74.6 ± 11.4 vs 60.1 ± 5.1 years; $p < 0.001$), whereas no significant differences were detected in body surface area or systolic and diastolic blood pressure values (Table 1). This age imbalance reflects the epidemiology of HFpEF as a predominantly age-associated syndrome. Although control subjects were within the older adult age range, the higher mean age of the HFpEF group should be considered when interpreting circulating biomarker levels, particularly LGALS3BP that is known to be associated with aging and inflammaging.

As expected, HFpEF patients showed a higher prevalence of cardiometabolic comorbidities, including arterial hypertension (76.1%), diabetes mellitus (44%), and dyslipidemia (62.4%), conditions rarely observed in the control group ($p < 0.001$). Smoking habit was also more common among patient group compared with controls (51.4% vs 8.2%; $p < 0.001$). Documented coronary artery disease (CAD) was present only in the patient group, including single-, double-, and triple-vessel disease, with a notable proportion of patients presenting triple-vessel involvement ($p < 0.001$). Consistently, coronary revascularization procedures, including percutaneous coronary intervention (30.3%; $p < 0.001$) and coronary artery bypass grafting (12.9%; $p = 0.008$) were reported exclusively in the patient group (Table 1). HFpEF patients also showed a greater use of guideline-directed cardiovascular therapies, including beta-blockers, ACE inhibitors/ARBs, and mineralocorticoid receptor antagonists (MRA) ($p < 0.001$). Functional status, assessed by World Health Organization functional class (WHO-FC), differed significantly between groups ($p < 0.001$), with HFpEF patients presenting a broader distribution across functional classes, whereas control subjects were limited to WHO-FC I–II (Table 1). Clinical signs of systemic congestion were present only in the HFpEF group. Peripheral edema was reported in 34.9% of patients, reflecting right-sided cardiac involvement. In contrast, left-sided symptoms (asthenia and/or dyspnea) and combined right- and left-sided signs were not observed in controls ($p < 0.001$) (Table 1).

Atrial fibrillation was also significantly more prevalent in patients, both in its paroxysmal form (15.6%) and, more prominently, in its chronic form (35.8%), whereas it was absent in the control group ($p = 0.003$ and $p < 0.001$, respectively) (Table 1).

Laboratory findings

From a laboratory standpoint, patients exhibited higher levels of NT-proBNP (2851.2 ± 1565.5 vs 156 ± 85.2 pg/mL; $p < 0.001$) and C-reactive protein (2.9 ± 4.5 vs 0.31 ± 0.33 mg/dL; $p < 0.001$), indicating both increased cardiac stress and systemic inflammation. Renal function was more impaired in patients compared to controls, as reflected by higher serum creatinine (1.45 ± 0.88 vs 1.14 ± 0.90 mg/dL; $p = 0.045$). Patients also showed higher serum sodium (138.9 ± 3.9 vs 136.7 ± 4.3 mEq/L; $p = 0.001$) and potassium levels (4.12 ± 0.59 vs 3.78 ± 0.43 mEq/L; $p < 0.001$). Notably, liver function indices were elevated in the HFpEF group compared to controls, with higher aspartate aminotransferase (AST) levels (48.2 ± 124.4 vs 19.6 ± 4.8 U/L; $p = 0.021$) and alanine aminotransferase (ALT) levels (40.9 ± 92.3 vs 17.0 ± 6.9 U/L; $p = 0.009$) (Table 1).

Echocardiographic analysis

Echocardiographic evaluation revealed structural and functional differences between HFpEF patients and control subjects. HFpEF patients showed greater indexed left ventricular mass (140.4 ± 55.9 vs 62.4 ± 9.8 g/m^2; $p < 0.001$) and increased interventricular septal thickness (11.5 ± 1.6 vs 10.3 ± 1.2 mm;

Table 1 Main demographics, clinical and laboratory characteristics

	Controls ($n=49$)	HFpEF patients ($n=109$)	p value
Demographics and risk factors			
Age, years	60.1 ± 5.1	74.6 ± 11.4	< 0.001
Male sex, n (%)	27 (55.1)	65 (59.6)	0.593
Body surface area, m^2	1.90 ± 0.22	1.91 ± 0.24	0.691
SBP, mmHg	128.5 ± 10.2	130.2 ± 15.4	0.450
DBP, mmHg	78.2 ± 6.5	77.8 ± 9.1	0.760
Arterial hypertension, n (%)	0 (0)	83 (76.1)	< 0.001
Smoking (Current/Former), n (%)	4 (8.2)	56 (51.4)	< 0.001
CAD family history, n (%)	5 (10.2)	42 (38.5)	< 0.001
Diabetes mellitus, n (%)	0 (0)	48 (44.0)	< 0.001
Dyslipidemia, n (%)	0 (0)	68 (62.4)	< 0.001
Co-morbidities			
Paroxysmal atrial fibrillation, n (%)	0 (0)	22 (20.2)	< 0.001
Permanent atrial fibrillation, n (%)	0 (0)	18 (16.5)	< 0.001
Single-vessel disease, n (%)	0 (0)	12 (11.0)	< 0.001
Double-vessel disease, n (%)	0 (0)	18 (16.5)	< 0.001
Triple-vessel disease, n (%)	0 (0)	24 (22.0)	< 0.001
Prior PCI, n (%)	0 (0)	33 (30.3)	< 0.001
Prior CABG, n (%)	0 (0)	14 (12.9)	< 0.001
Prior vascular surgery, n (%)	0 (0)	9 (8.3)	< 0.001
Prior Stroke/TIA, n (%)	0 (0)	11 (10.1)	< 0.001
COPD, n (%)	1 (2.0)	28 (25.7)	< 0.001
Thyroid disease, n (%)	2 (4.1)	15 (13.8)	0.062
Mild renal failure, n (%)	4 (8.2)	45 (41.3)	< 0.001
Severe renal failure, n (%)	0 (0)	8 (7.3)	0.040
Paroxysmal atrial fibrillation, n (%)	0 (0)	22 (20.2)	< 0.001
Permanent atrial fibrillation, n (%)	0 (0)	18 (16.5)	< 0.001
Left HF signs, n (%)	0 (0)	52 (47.7)	< 0.001
Right HF signs, n (%)	0 (0)	38 (34.9)	< 0.001
Any HF sign, n (%)	0 (0)	71 (65.1)	< 0.001
Laboratory parameters			
Potassium, mEq/L	3.78 ± 0.43	4.12 ± 0.59	< 0.001
NT-proBNP, pg/mL	156 ± 85	2851 ± 1565	< 0.001
C-reactive protein, mg/dL	0.31 ± 0.33	2.90 ± 4.46	< 0.001
Serum creatinine, mg/dL	1.14 ± 0.90	1.45 ± 0.88	0.045
AST, U/L	19.6 ± 4.8	48.2 ± 124.4	0.021
ALT, U/L	17.0 ± 6.9	40.9 ± 92.3	0.009
Medications			
Beta-blockers, n (%)	2 (4.1)	78 (71.6)	< 0.001
ACEi/ARB, n (%)	3 (6.1)	65 (59.6)	< 0.001
MRA, n (%)	0 (0)	35 (32.1)	< 0.001
HF specific therapy, n (%)	0 (0)	89 (81.7)	< 0.001

ACEi angiotensin-converting enzyme inhibitors, *ARB* angiotensin II receptor blockers, *CABG* coronary artery bypass grafting, *CAD* coronary artery disease, *COPD* chronic obstructive pulmonary disease, *HFpEF* heart failure with preserved ejection fraction, *MRA* mineralocorticoid receptor antagonists, *PCI* percutaneous coronary intervention, *TIA* transient ischemic attack, *ALT* alanine aminotransferase, *AST* aspartate aminotransferase, *BSA* body surface area, *HFpEF* heart failure with preserved ejection fraction

$p < 0.001$). Epicardial fat thickness was also higher in the HFpEF group compared with controls (3.68 ± 1.9 vs 2.98 ± 1.4 mm; p = 0.029). Although left ventricular ejection fraction remained within the preserved range in HFpEF patients, it was slightly lower compared with controls (LVEF 55.8 ± 5.32% vs 60.3 ± 2.8%; $p < 0.001$). Markers of diastolic dysfunction were more prominent in HFpEF patients, including increased left atrial diameter (LAD: 50.38 ± 10.43 vs 33.8 ± 2.6 mm; $p < 0.001$) and elevated filling pressures (E/A ratio: 16.5 ± 3.8 vs 7.0 ± 1.9; $p < 0.001$).

Evidence of right heart involvement was also observed in HFpEF patients. Systolic pulmonary artery pressure was higher compared with controls (39 ± 13.8 vs 28 ± 3.6 mmHg; $p < 0.001$), together with increased right atrial area (21.20 ± 7.3 vs 16.4 ± 2.4 cm2; $p < 0.001$). Right ventricular systolic function appeared reduced in HFpEF patients, as indicated by lower tricuspid annular plane systolic excursion (TAPSE: 18.4 ± 3.88 vs 23.7 ± 3.3 mm; $p < 0.001$) and fractional area change (FAC: 37.1 ± 12% vs 49.8 ± 15.1%; $p < 0.001$).. Consistent with these findings, right ventricle–pulmonary artery coupling was reduced in patients compared with controls (TAPSE/PAPs 0.55 ± 0.25 vs 0.85 ± 0.16; $p < 0.001$).

Valvular assessment revealed a different distribution between groups. Patients showed a higher prevalence of moderate-to-severe mitral regurgitation (moderate 33.9%, severe 1.8%), which was not observed in controls ($p < 0.001$). Similarly, moderate-to-severe tricuspid regurgitation was significantly more frequent among HFpEF patients (moderate 20.2%, severe 8.3%) compared with controls (moderate 2.0%, severe 0%; $p < 0.001$). Consistent with these alterations, HFpEF patients showed a higher echocardiographic probability of pulmonary hypertension (intermediate 44%, high 17%; $p < 0.001$). Inferior vena cava assessment showed larger mean diameters in patients compared to controls (18.3 ± 4.7 vs 16.2 ± 2.0 mm; p = 0.001), together with reduced collapsibility, findings consistent with increased systemic venous pressure (Table 2).

Proteomic profiling identifies LGALS3BP as a HFpEF-associated protein

Mass spectrometry-based proteomic analysis (LC–MS/MS) was performed on pooled plasma samples to compare the circulating proteome of HFpEF patients' proteome with that of control group matched for sex, age, and BMI. As shown in the Venn diagram (Fig. 1A), most proteins were detected in both groups, with 113 (91.13%) proteins shared between the two groups. A smaller subset of proteins was detected exclusively in one of the two groups, including 4 proteins (3.23%) unique to controls and 7 proteins (5.65%) uniquely detected in HFpEF samples (Table 3).

Among these proteins, LGALS3BP was detected exclusively in the HFpEF group, showing a markedly higher abundance compared with controls (abundance ratio = 100) (see red form protein of Fig. 1E and Table 3). To further evaluate this observation, circulating LGALS3BP levels were measured by ELISA in an independent cohort of plasma samples obtained from HFpEF patients (n = 75) and control subjects (n = 50). This analysis confirmed significantly higher LGALS3BP concentrations in HFpEF patients compared with controls (Fig. 1 B, $p < 0.0001$ vs control). Mean circulating LGALS3BP levels were 8.65 ± 0.66 ng/mL in HFpEF patients and 2.36 ± 0.26 ng/mL in control subjects. These findings support an association between increased circulating LGALS3BP levels and the HFpEF clinical phenotype. Proteomics analysis also revealed broader differences in protein expression between the two groups. Volcano Plot representation (Fig. 1C) identified 49 significantly modulated proteins, including 30 up-regulated and 19 down-regulated proteins in HFpEF compared with controls ($p < 0.05$). The list of significantly modulated proteins is reported in Table 4. To explore potential biological pathways associated with these proteomic changes, the dataset was analyzed using Ingenuity Pathway Analysis (IPA). The graphical summary (Fig. 1D) suggested activation of several upstream regulators related to inflammatory signaling, including nitric oxide synthase type 2 (NOS2), interferon-γ (IFN-γ), interleukin-6 (IL-6), and oncostatin M (OSM) (z-score > 2.0). These predicted upstream regulators were associated with downstream pathways related to immune cell chemotaxis and inflammatory responses. In parallel, predicted downregulation of anti-inflammatory pathways was observed, including interleukin-10 receptor subunit alpha (IL10RA; z-score = −2.65) and the Liver X Receptor-Retinoid X Receptor

Table 2 Continuous echocardiographic parameters

	Controls ($n=49$)		HFpEF patients ($n=109$)	p value
LVEDD, mm	44.2 ± 3.5		46.8 ± 5.1	0.002
LVESD, mm	28.1 ± 2.8		30.4 ± 4.6	0.001
LV mass index, g/m2	62.4 ± 9.8		140.4 ± 55.9	< 0.001
LAV index, mL/m2	23.7 ± 3.4		45.5 ± 19.2	< 0.001
LVEF, %	60.3 ± 2.8		55.8 ± 5.3	< 0.001
Epicardial fat thickness, mm	4.2 ± 1.1		6.8 ± 1.9	< 0.001
E/e' average	7.0 ± 1.9		16.5 ± 3.8	< 0.001
Eccentricity index	1.02 ± 0.04		1.25 ± 0.18	< 0.001
RVEDA, cm2	16.4 ± 2.4		21.2 ± 7.3	< 0.001
RVESA, cm2	6.2 ± 1.4		13.7 ± 5.1	< 0.001
RV basal diameter, mm	32.4 ± 3.8		41.2 ± 6.2	< 0.001
RV mid-cavity diameter, mm	26.1 ± 3.1		34.5 ± 5.4	< 0.001
RV longitudinal diameter, mm	65.2 ± 6.1		74.8 ± 9.3	< 0.001
Proximal RVOT (PLAX), mm	24.8 ± 3.2		31.4 ± 5.8	< 0.001
Right atrial area, cm^2	16.4 ± 2.4		21.2 ± 7.3	< 0.001
sPAP, mmHg	28.1 ± 3.6		39.0 ± 13.8	< 0.001
TAPSE, mm	23.7 ± 3.3		18.4 ± 3.9	< 0.001
Fractional area change, %	49.8 ± 15.1		37.1 ± 12.0	< 0.001
TAPSE/sPAP ratio	0.85 ± 0.16		0.55 ± 0.25	< 0.001
IVC diameter, mm	16.2 ± 2.0		18.3 ± 4.7	0.001
MR Absent/Trivial, n (%)	46 (93.9)		28 (25.7)	< 0.001
MR Mild, n (%)	3 (6.1)		42 (38.5)	< 0.001
MR Moderate, n (%)	0 (0)		26 (23.9)	< 0.001
MR Severe, n (%)	0 (0)		13 (11.9)	< 0.001
TR Absent/Trivial, n (%)	42 (85.7)		32 (29.4)	< 0.001
TR Mild, n (%)	6 (12.3)		46 (42.2)	< 0.001
TR Moderate, n (%)	1 (2.0)		22 (20.2)	< 0.001
TR Severe, n (%)	0 (0)		9 (8.2)	< 0.001
IVC Collapsibility < 50%, n (%)		1 (2.0)	41 (37.6)	< 0.001
PH Prob—Low, n (%)	47 (95.9)		35 (32.1)	< 0.001
PH Prob—Intermediate, n (%)	2 (4.1)		44 (40.4)	< 0.001
PH Prob—High, n (%)	0 (0)		30 (27.5)	< 0.001

E/e' ratio of transmitral flow velocity to early diastolic velocity of the mitral annulus, *FAC* fractional area change, *HFpEF* heart failure with preserved ejection fraction, *LVEDD* left ventricular end-diastolic diameter, *LVESD* left ventricular end-systolic diameter, *PLAX* parasternal long-axis view, *RVEDA* right ventricular end-diastolic area, *RVESA* right ventricular end-systolic area, *RVOT* right ventricular outflow tract, *sPAP* systolic pulmonary artery pressure, *TAPSE* tricuspid annular plane systolic excursion, *TAPSE/sPAP* right ventricular–pulmonary artery coupling index, *LV* left ventricular, *LVEF* left ventricular ejection fraction, *MR* mitral regurgitation, *PH* pulmonary hypertension, *TR* tricuspid regurgitation, *VCI* vena cava inferior

(LXR/RXR) activation pathway (z-score = − 1.66). A more detailed network analysis highlighting LGALS3BP-associated interactions is presented in Fig. 1E. In this network, NOS2 was predicted as an activated upstream regulator (z-score = 2.45), with several proteins contributing to this predicted activation, including LGALS3BP, which was detected exclusively in HFpEF plasma samples (see color red and abundance ratio = 100). Ingenuity Pathway Analysis results are predictive and should be interpreted as hypothesis-generating rather than definitive evidence of pathway activation.

eNOS deficiency is associated with altered LGALS3BP expression and isoform pattern in endothelial cells

Based on the plasma proteomic signature observed in HFpEF patients, including the predicted activation of inflammatory and metabolic pathways highlighted by IPA, with NOS2 identified as a predicted upstream regulator (Fig. 1E), we established an in vitro model to investigate whether metabolic stress influences LGALS3BP expression in endothelial cells and whether eNOS deficiency modifies this response.

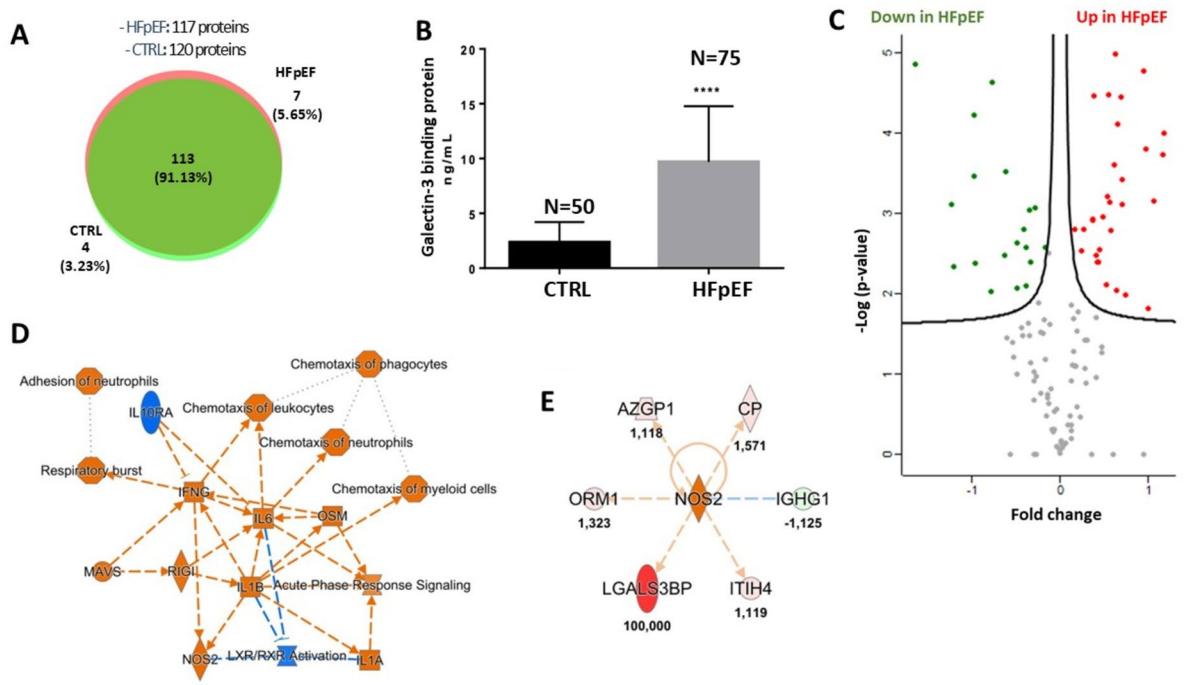

Fig. 1 Proteomic profiling of HFpEF patients. (**A**) Venn Diagram of robustly quantified proteins in HFpEF patients and control subjects. (**B**) Serum levels of galectin-3-binding protein (LGALS3BP) measured by ELISA in control subjects and HFpEF patients. HFpEF patients exhibit significantly higher circulating LGALS3BP concentrations compared with controls. **** $p < 0.0001$ vs control, one-way ANOVA (Tukey post-hoc)Serum levels of galectin-3-binding protein (LGALS3BP) measured by ELISA in control subjects and HFpEF patients. HFpEF patients exhibit significantly higher circulating LGALS3BP concentrations compared with controls. **** $p < 0.0001$ vs control, one-way ANOVA (Tukey post-hoc). (**C**) Volcano plot showing the distribution of differentially expressed proteins identified by LC–MS/MS analysis. Grey dots indicate proteins not differentially expressed, green dots represent the significant downregulated proteins, and red dots indicate the significant upregulated proteins in HFpEF patients compared with controls. ((**D**) IPA graphical summary showing the upregulated (in orange) and downregulated (in blue) nodes of interconnected upstream regulators and biological functions in HFpEF patients compared with controls. (**E**) IPA network underlines the significant activation of nitric oxide synthase 2 *(NOS2)* as upstream regulator in HFpEF subjects exploited by five proteins including LGALS3BP. Green and red forms indicate the proteins quantified by LC–MS/MS in terms of down- and up-regulated proteins in HFpEF plasma sample, respectively. Protein ratios (HFpEF Vs CTRL) were reported under each protein. Rhombus form stand s for enzyme, trapezoid form symbolizes a trasporter, ellipse form a trasmembrane receptor, and, finally, circlers represent other proteins. Results are reported as mean ± SD. Statistical analysis was performed by one-way ANOVA with Tukey test for multiple comparisons; **** $p < 0.0001$ vs control (CT)

Murine aortic endothelial cells derived from wild-type (WT) mice (Fig. 2) and eNOS knock-out (eNOS KO) mice (Fig. 3) were exposed to basal conditions, high glucose (HG), high insulin (HI), or combined HG + HI treatment to reproduce aspects of metabolic stress and hyperinsulinemia frequently associated with HFpEF. In WT endothelial cells, western blot analysis indicated that insulin signaling remained predominantly oriented toward the metabolic pathway. Under combined HG + HI stimulation, the phosphorylated AKT/AKT ratio increased markedly (approximately 18-fold relative to basal conditions) (Fig. 2A), whereas the phosphorylated eNOS/eNOS ratio decreased (approximately 4.5-fold relative to basal) (Fig. 2B). These findings may reflect compensatory activation of AKT signaling under conditions of reduced eNOS activity. A modest increase in ERK phosphorylation was observed (Fig. 2C), while VCAM-1 expression, an established marker of endothelial inflammatory activation, showed only a mild and non-significant increase (approximately 1.2-fold relative to basal) (Fig. 2D). In WT endothelial

Table 3 List of proteins uniquely quantified in plasma samples

Protein IDs	Gene names	Description	HFpEF	CTRL
P02741	CRP	C-reactive protein	+	
P06702	S100A9	Protein S100-A9	+	
PODJI8	SAA1	Serum amyloid protein A	+	
P18428	LBP	Lipopolysaccharide-bidning protein	+	
P20742	PZP	Pregnancy zone protein	+	
Q08380	**LGALS3BP**	**Galectin-3 binding protein**	**+**	
Q9NZP8	C1RL	Complement C1r subcomponent-like protein	+	
A0A0J9YY99		Ig heavy chain V-III region CAM		+
O95445	APOM	Apolipoprotein M		+
P01742	IGHV1-69–2	Ig heavy chain V-I region EU		+
Q16610	ECM1	Extracellular matrix protein 1		+

The sign "+" indicates the clinical condition in which the protein was robustly quantified

cells, western blot analyses revealed that insulin signaling remained predominantly oriented towards the metabolic pathway. Under combined HG + HI stimulation, the phosphorylated AKT/AKT ratio increased markedly (approximately 18-fold relative to basal conditions) (Fig. 2 A), whereas the phosphorylated eNOS/eNOS ratio decreased (approximately 4.5-fold relative to basal) (Fig. 2B). These findings may reflect compensatory activation of AKT signaling under conditions of reduced eNOS activity. A modest increase in ERK phosphorylation was observed (Fig. 2C), while VCAM-1 expression, an established marker of endothelial inflammatory activation, showed only a mild and non-significant increase (approximately 1.2-fold relative to basal) (Fig. 2D). In contrast, eNOS KO endothelial cells exhibited a pro-inflammatory signaling profile. VCAM-1 expression was substantially higher than in WT cells and increased significantly under HI and combined HG + HI (1.8-fold with HI alone and 3.5-fold with HG + HI) (Fig. 3 C), whereas pERK and ERK expressions were unchanged (Fig. 3B). In addition, AKT phosphorylation was not detected in eNOS-deficient cells (Fig. 2A), indicating disruption of the canonical insulin signaling pathway in this model. These alterations are consistent with impaired nitric oxide signaling and endothelial dysfunction characteristic of HFpEF. We next examined LGALS3BP expression under these conditions. In WT endothelial cells, western blot analysis revealed a predominant LGALS3BP band at approximately 100 (−150) kDa, corresponding to the expected full-length protein (Fig. 2E). In WT cells, full-length LGALS3BP expression showed a modest and non-significantly increased under HG (1.28-fold relative to basal) and HI (1.20-fold relative to basal) conditions, with the largest trend observed under combined HG + HI treatment (2.68-fold relative to basal) (Fig. 2F). In eNOS KO cells, full-length LGALS3BP expression showed a more limited increase under metabolic stress, with a moderate but statistically significant upregulation observed under HG + HI treatment (1.44-fold compared with basal conditions; $p < 0.05$) (Fig. 3E). Notably, western blot analysis consistently revealed an additional lower-molecular weight LGALS3BP band (~ 50–70 kDa) in eNOS-deficient cells (Fig. 3 D, F), which was minimally detectable or absent in WT cells. Densitometric analysis indicated that this lower-molecular weight LGALS3BP formwas consistently enriched in eNOS KO cells under metabolic stress conditions, reaching approximately a twofold increase relative to basal levels. Statistical comparison further revealed a significant difference in full-length LGALS3BP expression between WT and eNOS KO cells under combined HG + HI treatment ($p < 0.05$), while the lower-molecular weight LGALS3BP form was selectively observed in eNOS-deficient cells. Overall, these findings indicate that eNOS deficiency is associated with an altered LGALS3BP expression profile under metabolic stress, characterized by a modest increase in the full-length protein and the presence of a lower-molecular weight LGALS3BP isoform.

PNGase F treatment reveals altered LGALS3BP processing in eNOS-deficient cells

To investigate whether the differences in LGALS3BP molecular weight observed between WT and eNOS

Table 4 List of significantly differential expressed proteins in HFpEF plasma samples

Protein IDs	Gene names	Description	Expression in HFpEF
P02766	TTR	Transthyretin	down
P02753	RBP4	Retinol-binding protein 4	down
P35858	IGFALS	Insulin-like growth factor-binding protein complex acid labile subunit	down
P06727	APOA4	Apolipoprotein A-IV	down
P01861	IGHG4	Ig gamma-4 chain C region	down
P02765	AHSG	Alpha-2-HS-glycoprotein	down
P02652	APOA2	Apolipoprotein A-II	down
P02647	APOA1	Apolipoprotein A-I	down
P04196	HRG	Histidine-rich glycoprotein	down
P00748	F12	Coagulation factor XII	down
P43652	AFM	Afamin	down
P29622	SERPINA4	Kallistatin	down
P27169	PON1	Serum paraoxonase/arylesterase 1	down
A0A0A0MRZ8	IGKV3D-11	Ig kappa chain V-III region VG	down
P01008	SERPINC1	Antithrombin-III	down
P02774	GC	Vitamin D-binding protein	down
P19823	ITIH2	Inter-alpha-trypsin inhibitor heavy chain H2	down
P02790	HPX	Hemopexin	down
P01857	IGHG1	Ig gamma-1 chain C region	down
Q14624	ITIH4	Inter-alpha-trypsin inhibitor heavy chain H4	up
P06681	C2	Complement C2	up
P02649	APOE	Apolipoprotein E	up
P07358	C8B	Complement component C8 beta chain	up
P0C0L5	C4B	Complement C4-B	up
Q13790	APOF	Apolipoprotein F	up
P68871	HBB	Hemoglobin subunit beta	up
P07357	C8A	Complement component C8 alpha chain	up
P02743	APCS	Serum amyloid P-component	up
P02760	AMBP	Protein AMBP	up
P0DP08	IGHV4-61	Ig heavy chain V-II region NEWM	up
P00915	CA1	Carbonic anhydrase 1	up
P05155	SERPING1	Plasma protease C1 inhibitor	up
P00751	CFB	Complement factor B	up
P01031	C5	Complement C5	up
P04003	C4BPA	C4b-binding protein alpha chain	up
P02675	FGB	Fibrinogen beta chain	up
P01009	SERPINA1	Alpha-1-antitrypsin	up
P02746	C1QB	Complement C1q subcomponent subunit B	up
P00450	CP	Ceruloplasmin	up
P02679	FGG	Fibrinogen gamma chain	up
P02747	C1QC	Complement C1q subcomponent subunit C	up
P02671	FGA	Fibrinogen alpha chain	up
P09871	C1S	Complement C1s subcomponent	up
P00738	HP	Haptoglobin	up

Table 4 (continued)

Protein IDs	Gene names	Description	Expression in HFpEF
P01011	SERPINA3	Alpha-1-antichymotrypsin	up
Q06033	ITIH3	Inter-alpha-trypsin inhibitor heavy chain H3	up
P02750	LRG1	Leucine-rich alpha-2-glycoprotein	up
P10643	C7	Complement component C7	up
P02748	C9	Complement component C9	up
A0A0C4DH38	IGHV5-51	Immunoglobulin heavy variable 5–51	up
P02766	TTR	Transthyretin	up
P02753	RBP4	Retinol-binding protein 4	up
P35858	IGFALS	Insulin-like growth factor-binding protein complex acid labile subunit	up
P06727	APOA4	Apolipoprotein A-IV	up
P01861	IGHG4	Ig gamma-4 chain C region	up
P02765	AHSG	Alpha-2-HS-glycoprotein	up
P02652	APOA2	Apolipoprotein A-II	up
P02647	APOA1	Apolipoprotein A-I	up
P04196	HRG	Histidine-rich glycoprotein	up
P00748	F12	Coagulation factor XII	up
P43652	AFM	Afamin	up
P29622	SERPINA4	Kallistatin	up
P27169	PON1	Serum paraoxonase/arylesterase 1	up
A0A0A0MRZ8	IGKV3D-11	Ig kappa chain V-III region VG	up
P01008	SERPINC1	Antithrombin-III	up
P02774	GC	Vitamin D-binding protein	up
P19823	ITIH2	Inter-alpha-trypsin inhibitor heavy chain H2	up
P02790	HPX	Hemopexin	up
P01857	IGHG1	Ig gamma-1 chain C region	up
Q14624	ITIH4	Inter-alpha-trypsin inhibitor heavy chain H4	up
P06681	C2	Complement C2	up
P02649	APOE	Apolipoprotein E	up
P07358	C8B	Complement component C8 beta chain	up
P0C0L5	C4B	Complement C4-B	up
Q13790	APOF	Apolipoprotein F	up
P68871	HBB	Hemoglobin subunit beta	up
P07357	C8A	Complement component C8 alpha chain	up
P02743	APCS	Serum amyloid P-component	up
P02760	AMBP	Protein AMBP	up
P0DP08	IGHV4-61	Ig heavy chain V-II region NEWM	up
P00915	CA1	Carbonic anhydrase 1	up
P05155	SERPING1	Plasma protease C1 inhibitor	up
P00751	CFB	Complement factor B	up
P01031	C5	Complement C5	up
P04003	C4BPA	C4b-binding protein alpha chain	up
P02675	FGB	Fibrinogen beta chain	up
P01009	SERPINA1	Alpha-1-antitrypsin	up
P02746	C1QB	Complement C1q subcomponent subunit B	up

Table 4 (continued)

Protein IDs	Gene names	Description	Expression in HFpEF
P00450	CP	Ceruloplasmin	up
P02679	FGG	Fibrinogen gamma chain	up
P02747	C1QC	Complement C1q subcomponent subunit C	up
P02671	FGA	Fibrinogen alpha chain	up
P09871	C1S	Complement C1s subcomponent	up
P00738	HP	Haptoglobin	up
P01011	SERPINA3	Alpha-1-antichymotrypsin	up
Q06033	ITIH3	Inter-alpha-trypsin inhibitor heavy chain H3	up
P02750	LRG1	Leucine-rich alpha-2-glycoprotein	up
P10643	C7	Complement component C7	up
P02748	C9	Complement component C9	up
A0A0C4DH38	IGHV5-51	Immunoglobulin heavy variable 5–51	up

In the column "Expression in HFpEF" is indicated the modulation. The down- and up-regulated proteins correspond to the green and red dots of Volcano Plot (Fig. 1C), respectively

KO endothelial cells were related to glycosylation status or abnormal protein processing, deglycosylation assays were performed, followed by Western blot analysis. In WT cells, PNGase F treatment resulted in the detection of both a higher-molecular-weight LGALS3BP band (~ 100 kDa) and the lower-molecular-weight form (~ 50–70 kDa) (Fig. 4 A). This pattern is consistent with the presence of multiple LGALS3BP species that may reflect different glycosylation states or processing forms. In contrast, in eNOS KO MAECs, only the lower-molecular-weight LGALS3BP band was detected both before and after PNGase F treatment (Fig. 4B). The persistence of this band following enzymatic deglycosylation suggests that the reduced molecular weight observed in eNOS-deficient cells cannot be explained solely by differences in N-linked glycosylation.

In contrast, in eNOS KO cells, only the lower-molecular-weight LGALS3BP band was detected both before and after PNGase F treatment (Fig. 4 B). The persistence of this band following enzymatic deglycosylation suggests that the reduced molecular weight observed in eNOS-deficient cells cannot be explained solely by differences in N-linked glycosylation. Overall, these findings indicate that eNOS deficiency is associated with an altered LGALS3BP molecular profile in endothelial cells. Although the precise biochemical nature of this lower-molecular-weight form remains to be determined, the data are consistent with altered processing or stability of LGALS3BP under conditions of impaired eNOS signaling.

Metabolic stress is associated with increased autophagy and senescence in eNOS-deficient endothelial cells

To explore cellular responses occurring in parallel with altered LGALS3BP expression and eNOS deficiency under metabolic stress conditions, autophagic activity and cellular senescence were evaluated in WT and eNOS KO endothelial cells exposed to basal conditions, HG, HI and combined HG + HI treatments.

Autophagic activity was evaluated using fluorescence-based LC3 staining. LC3-positive autophagosomes were visualized as green fluorescent puncta, while nuclei were counterstained with DAPI (blue)., Fluorescence microscopy revealed an increased number of in autophagosomes in eNOS KO cells compared with WT cells under all metabolic stress conditions. Representative images are shown in Fig. 5A, where autophagic structures are indicated

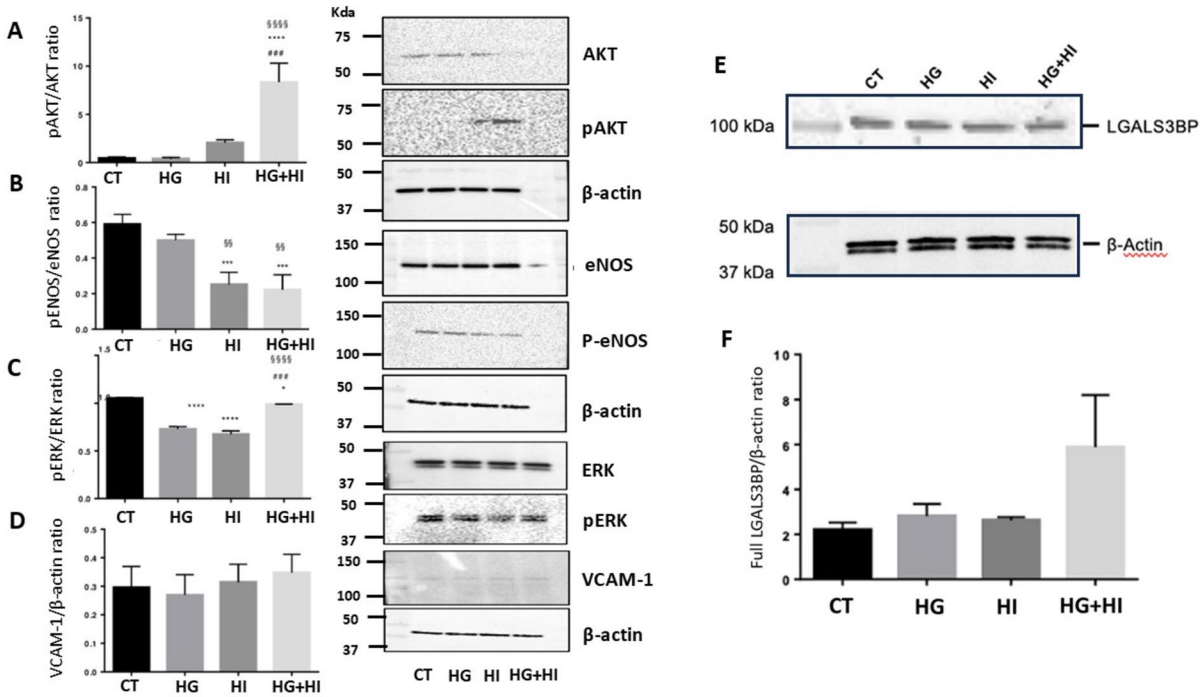

Fig. 2 Insulin signaling pathway and expression of full-length galectin-3 binding protein in wild-type murine aortic endothelial cells. (**A**-**D**) Representative Western blot images and densitometric quantification showing the expression of insulin signaling pathway components in wild-type murine aortic endothelial cells (MAEC WT) under basal (CT), high glucose (HG), high insulin (HI), and combined HG + HI conditions. Densitometric quantification of pAKT/AKT, p-eNOS/eNOS, pERK/ERK, and VCAM-1/β-actin expression is shown for MAEC WT. Data are reported as mean ± SD. Statistical analysis was performed by one-way ANOVA with Tukey test for multiple comparisons; *$p < 0.05$, **$p < 0.01$, ***$p < 0.001$, ****$p < 0.0001$ vs control (CT); §$p < 0.05$, §§ $p < 0.01$, §§§ $p < 0.001$, §§§ $p < 0.0001$ vs HG; #### $p < 0.0001$ vs HI. (**E**–**F**) Representative Western blot images and densitometric quantification showing LGALS3BP expression in MAEC WT under basal, high glucose (HG), high insulin (HI), and combined HG + HI conditions. The full-length LGALS3BP isoform (~ 100 kDa) is shown. (F) Densitometric quantification of full-length LGALS3BP normalized to β-actin in WT MAECs. Data are expressed as mean ± SD of fold change relative to basal conditions. Densitometric analyses were performed using ImageJ. Statistical analysis was done by one-way ANOVA with Tukey test for multiple comparisons; p = NS

by arrows. Quantitative analysis confirmed a higher percentage of autophagy-positive cells in eNOS KO culture compared to WT phenotype across all treatments (Fig. 5 B; $p < 0.0001$ vs control WT).

Cellular senescence was assessed by SA-β-gal staining. Senescent cells were identified by the presence of blue cytoplasmic staining. Consistent with autophagy results, eNOS KO culture exhibited a higher proportion of senescence-positive cells compared with WT phenotype under all metabolic stress conditions (Fig. 5 C). Quantitative analysis confirmed a significant increase in senescence-positive cells in eNOS KO culture across the experimental treatments (Fig. 5 D; $p < 0.0001$ vs control WT).

Discussion

The present study identifies LGALS3BP as a circulating protein significantly elevated in older HFpEF patients and associated with endothelial stress and metabolic dysfunction. By integrating plasma proteomic profiling with mechanistic analyses in MAECs, our findings suggest that alterations in nitric oxide signaling and metabolic stress responses induced by high glucose and insulin exposure may be linked to changes in LGALS3BP expression and processing.

Proteomic analysis revealed that LGALS3BP was selectively detected in the HFpEF plasma proteome and significantly elevated in an independent

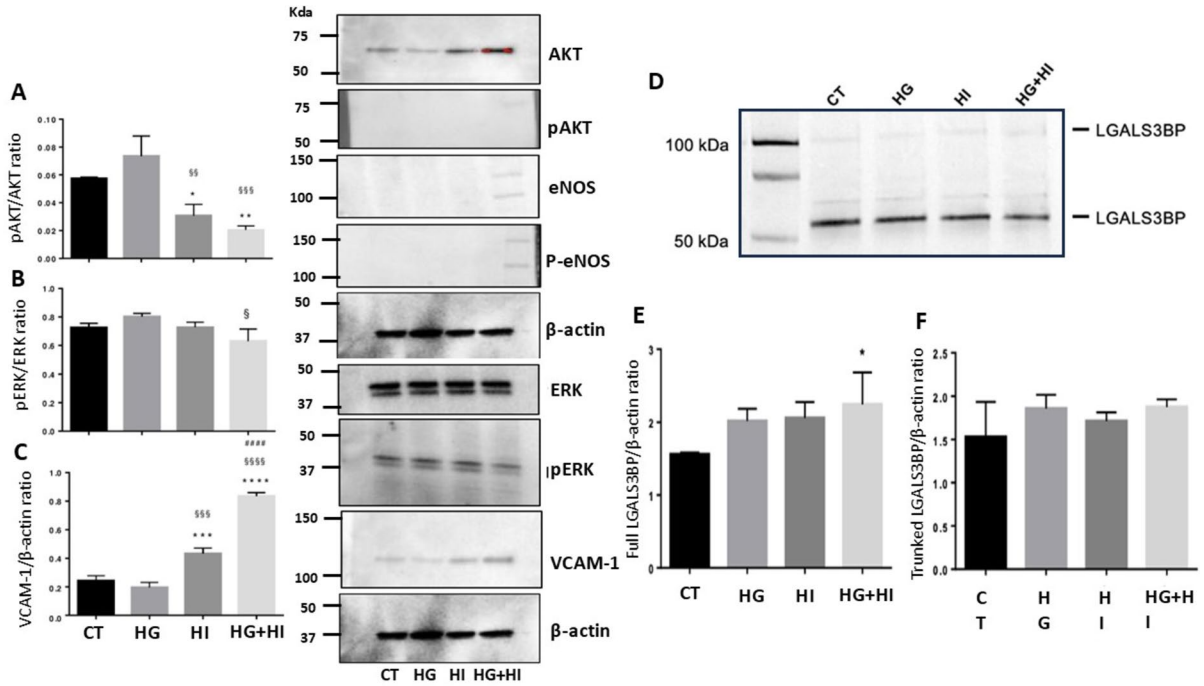

Fig. 3 eNOS deficiency is associated with altered LGALS3BP expression and isoform pattern under metabolic stress. (**A**-**C**) Representative Western blot images and densitometric quantification showing the expression of insulin signaling pathway components in murine aortic endothelial cells knock-out for eNOS (eNOS KO MAEC) under basal (CT), high glucose (HG), high insulin (HI), and combined HG + HI conditions. Densitometric quantification of pAKT/AKT, p-eNOS/eNOS, pERK/ERK, and VCAM-1/β-actin expression is shown for eNOS KO cells. Data are expressed as mean ± SD. Statistical analysis was performed by one-way ANOVA with Tukey test for multiple comparisons; *$p < 0.05$, **$p < 0.01$, ***$p < 0.001$, ****$p < 0.0001$ vs control (CT); §§ $p < 0.01$, §§§ $p < 0.001$, §§§ $p < 0.0001$ vs HG; #### $p < 0.0001$ vs HI. (**D**) Representative Western blot images showing LGALS3BP expression pattern in eNOS KO MAEC cells under basal, high glucose (HG), high insulin (HI) and combined HG + HI conditions. The full-length LGALS3BP isoform (~ 100 kDa) and the lower-molecular weight isoform (~ 50–70 kDa) are indicated. (E–F) Densitometric quantification of (**E**) full-length and (**F**) trunked (lower-molecular weight isoform) LGALS3BP normalized to β-actin in eNOS KO MAECs. Data are expressed as mean ± SD of fold change relative to basal conditions. Densitometric analyses were performed using ImageJ or Image Lab Software (Biorad). Statistical analysis was performed by one-way ANOVA with Tukey test for multiple comparisons; *$p < 0.05$ vs control (CT)

validation cohort. These observations are consistent with emerging evidence indicating that LGALS3BP is involved in inflammatory and extracellular matrix–related pathways associated with cardiovascular disease. Previous studies, indeed, have linked increased circulating LGALS3BP levels with myocardial fibrosis, impaired exercise capacity, and disease severity in HFpEF populations [3, 31].

Compared with previous literature describing LGALS3BP primarily as a downstream marker associated with inflammatory signaling and extracellular matrix remodeling [15, 16], our data provide novel mechanistic evidence linking its expression to endothelial nitric oxide synthase dysfunction and metabolic stress, thereby suggesting a potential role of LGALS3BP in endothelial maladaptation rather than being solely a passive disease marker.

Within the mechanistic framework proposed here, these alterations are interpreted as downstream consequences of endothelial dysfunction and metabolic stress rather than as primary drivers of disease development. In this context, dysregulation of LGALS3BP may influence galectin-mediated pathways downstream of nitric oxide imbalance, potentially contributing to phenotypes previously attributed primarily to galectin-3 alone. Notably, recent clinical evidence suggests that galectin-related pathways may be modifiable, as pharmacological interventions such as

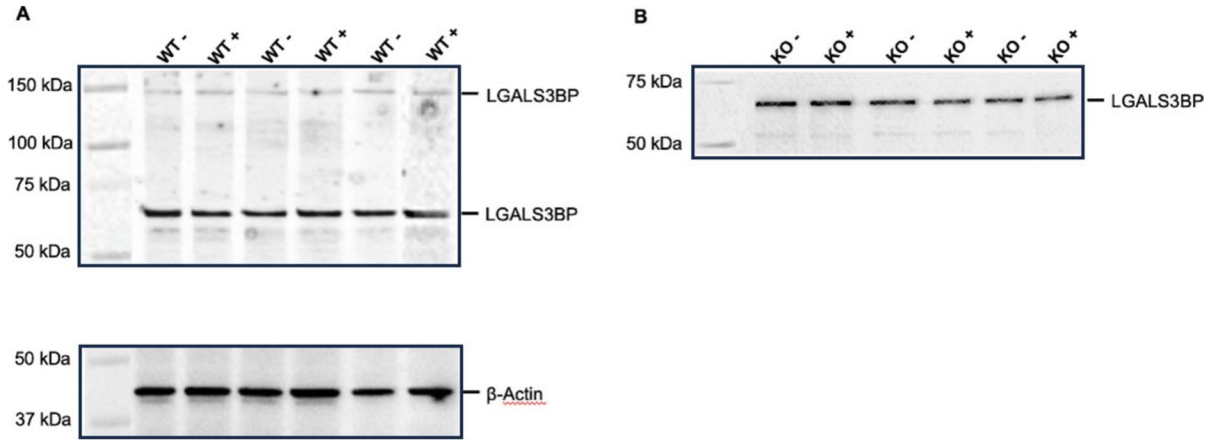

Fig. 4 PNGase F deglycosylation reveals altered LGALS3BP processing in eNOS knock-out murine aortic endothelial cells. Representative Western blot analysis of LGALS3BP expression following PNGase F treatment under denaturing conditions. (**A**) WT MAECs display both high-molecular-weight (~100 kDa) and low-molecular-weight (~50–70 kDa) LGALS3BP forms before (without PNGase F, WT-) and after (with PNGase F, WT+) deglycosylation. (**B**) eNOS KO MAECs show exclusive detection of the lower-molecular-weight LGALS3BP isoform (KO-) before and (KO+) after PNGase F treatment. β-actin was used as a loading control. Representative blots from three independent experiments are shown

SGLT2 inhibition have been shown to modulate circulating galectin-associated biomarkers in HFpEF populations [32].

Beyond its inflammatory role, LGALS3BP has been reported to influence endothelial biology, including VEGF-dependent angiogenic signaling, endothelial activation, and vascular remodeling [33]. Altered LGALS3BP expression has been described in vascular and cardiopulmonary diseases characterized by endothelial dysfunction and maladaptive remodeling [34, 35]. Consistent with these observations, our *in vitro* data show that endothelial cells exposed to metabolic stress conditions, such as high glucose or high insulin, exhibit features of endothelial stress, including increased autophagic activity, enhanced cellular senescence, and upregulation of adhesion molecules, particularly in the setting of eNOS deficiency. These findings support a model in which metabolic stress first disrupts endothelial nitric oxide signaling and is accompanied by alterations in LGALS3BP expression and processing. Within this context, LGALS3BP may represent part of a broader galectin-centered network linking metabolic stress to endothelial dysfunction and vascular remodeling in HFpEF. A notable observation of this study is that loss of eNOS activity was associated with alterations in LGALS3BP expression and molecular profile in endothelial cells. In eNOS-deficient cells exposed to metabolic stress, the induction of full-length LGALS3BP protein was reduced and accompanied by the accumulation of a a lower-molecular-weight LGALS3BP form. This lower-molecular-weight LGALS3BP band may reflect altered post-translational processing, including proteolytic cleavage, aberrant glycosylation-independent processing, or reduced protein stability under conditions of impaired nitric oxide signaling. Deglycosylation experiments using PNGase F suggested that this difference cannot be explained solely by changes in glycosylation status, indicating that additional mechanisms related to protein processing or stability may be involved. Given the central role of eNOS-derived nitric oxide in maintaining endothelial homeostasis, vascular tone, and anti-inflammatory signaling, our data are consistent with the possibility that nitric oxide signaling influences LGALS3BP expression or maturation. In parallel, bioinformatic pathway analysis of the plasma proteomic dataset suggested activation of NOS2-related inflammatory pathways in HFpEF patients [3, 35]. It should be emphasized that Ingenuity Pathway Analysis provides predictive, knowledge-based inference rather than direct experimental evidence; therefore, activation of NOS2-related pathways should be interpreted as hypothesis-generating. Taken together,

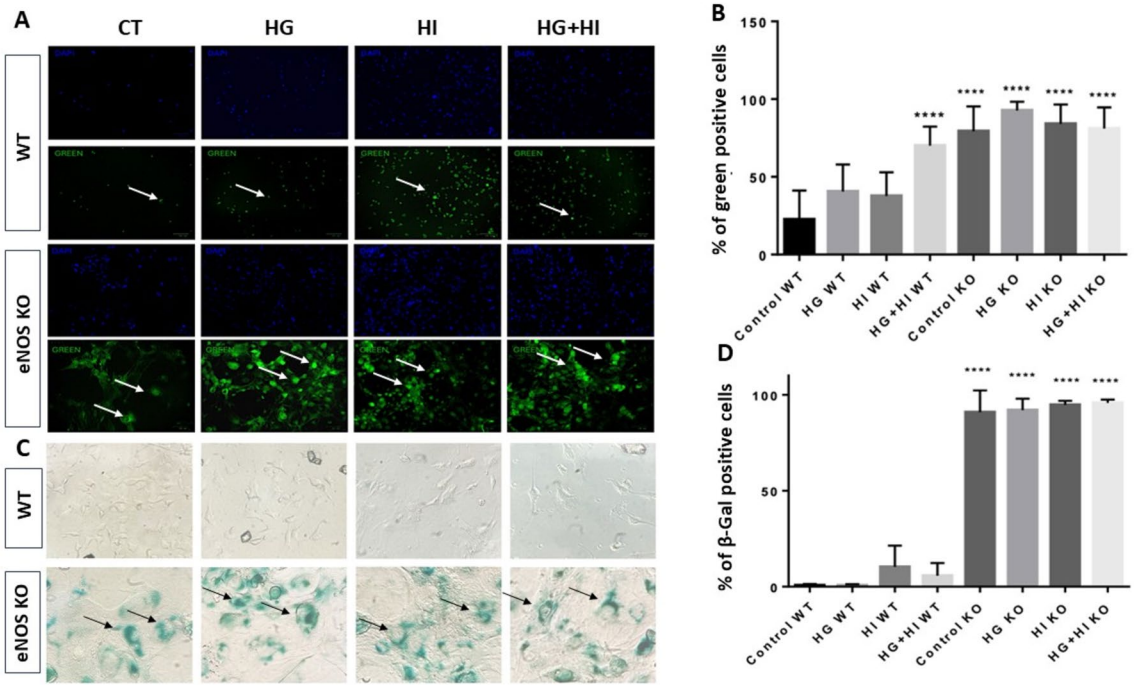

Fig. 5 Functional consequences of metabolic stress in wild type and eNOS knock-out murine aortic endothelial cells. (**A**) Representative fluorescence microscopy images of LC3-positive autophagosomes (green) and nuclei (blue) under basal, HG, HI, and HG + HI conditions in WT and KO cells. Arrows indicate autophagosomes. (**B**) Quantification of autophagy-positive cells expressed as mean ± SD of percentage of total cells eNOS KO MAEC shows significantly higher autophagy under all stress conditions. (**C**) Representative images of senescence-associated β-galactosidase (SA-β-gal) staining in WT and KO cells under the same conditions. (**D**) Quantification of senescence-positive cells expressed as mean ± SD of percentage of SA-β-gal positive cells. KO cells exhibit a marked increase in senescence across all metabolic stress treatments. Statistical analysis was performed by one-way ANOVA with Tukey test for multiple comparisons, ****$p < 0.0001$ vs control WT

these observations raise the possibility that dysregulation of the eNOS axis, including both eNOS signaling and compensatory NOS2 activation, may influence LGALS3BP processing and secretion in conditions of endothelial stress.

Altered LGALS3BP processing may in turn influence galectin-dependent signaling pathways that regulate endothelial inflammatory and structural responses under metabolic stress. However, the precise functional consequences of the lower-molecular-weight LGALS3BP form identified in eNOS-deficient cells remain to be determined and will require further investigation.

From a cellular perspective, eNOS deficiency was associated with altered endothelial stress responses in metabolically challenged cells. In our model, endothelial cells lacking eNOS exhibited increased markers of autophagy and cellular senescence compared with wild-type cells exposed to similar metabolic stress conditions. These findings are consistent with the concept that disruption of eNOS signaling alters endothelial stress-adaptive pathways due to the lack of uncoupled eNOS, which is a major enzymatic source of superoxide anion under pathological conditions [36]. The endothelial model used in this study does not reproduce the full complexity of HFpEF, as it lacks immune cell interactions, neurohormonal regulation, and systemic hemodynamic forces, which represent key contributors to disease pathophysiology.Previous studies have shown that changes in redox balance and antioxidant defenses can substantially influence reactive oxygen species production and cellular stress responses in endothelial cells exposed to chronic metabolic disturbances [37, 38]. Mitochondrial reactive oxygen species, in particular, contribute to endothelial redox imbalance

and reduced nitric oxide bioavailability, key mechanisms underlying microvascular dysfunction and vascular aging in cardiometabolic disease [39]. Although the precise mechanisms linking eNOS deficiency to these stress responses remain to be clarified, the present findings suggest that impaired nitric oxide signaling may contribute to the altered cellular phenotype observed in our model.

From a clinical perspective, the identification of LGALS3BP as a circulating protein elevated in HFpEF supports its potential relevance as a biomarker reflecting endothelial stress and metabolic dysregulation. Unlike conventional inflammatory markers that primarily reflect downstream inflammatory activity, LGALS3BP may capture alterations at the vascular interface linked to endothelial nitric oxide signaling and galectin-dependent pathways. Compared with established biomarkers such as NT-proBNP (hemodynamic stress marker) and C-reactive protein (systemic inflammation marker), LGALS3BP may provide complementary information reflecting endothelial dysfunction and extracellular matrix–immune interactions; however, its incremental clinical utility requires further validation in larger cohorts. Recent bioinformatic and clinical analyses further support LGALS3BP as a biomarker associated with coronary atherosclerosis and cardiovascular risk stratification [40], suggesting that its relevance may extend across multiple vascular disease states.

Several limitations should be acknowledged. First, the proteomic analysis was exploratory and based on pooled plasma samples, although key findings were validated by ELISA in an independent cohort. Second, the endothelial model used represents a simplified experimental system focused on nitric oxide–dependent endothelial stress and therefore does not fully reproduce the multifactorial pathophysiology of HFpEF in older patients in vivo. Accordingly, the mechanistic findings derived from this model should be interpreted within this experimental context. Third, the present data demonstrate associations between metabolic stress, eNOS deficiency, and LGALS3BP alterations but do not establish direct causal mechanisms. An additional limitation is the significant age difference between HFpEF patients and controls, which may have influenced LGALS3BP levels given its known association with aging-related inflammatory processes (inflammaging). Although control subjects were within the older adult age range, the higher mean age observed in the HFpEF cohort reflects the age-dependent epidemiology of the syndrome. Importantly, the magnitude of the observed increase in circulating LGALS3BP suggests the presence of a disease-related endothelial stress signal beyond aging alone. Future studies will be required to determine whether LGALS3BP actively contributes to endothelial dysfunction or primarily reflects vascular stress responses.

In conclusion, our study identifies LGALS3BP as a circulating protein associated with endothelial dysfunction in older patients with HFpEF and suggests an unexpected potential link between impaired nitric oxide signaling and LGALS3BP processing under metabolic stress conditions. By integrating clinical proteomic data with mechanistic endothelial models, this work provides a framework linking metabolic stress, endothelial nitric oxide synthase signaling, LGALS3BP alterations, and endothelial stress responses in HFpEF. Although our data support an association between elevated LGALS3BP levels and endothelial dysfunction, they do not establish a causal role for LGALS3BP in disease progression. Further studies are required to clarify its functional relevance and potential utility for patient stratification and therapeutic monitoring in HFpEF.

Authors' Contribution R.M. conceived the project, designed the study, supervised and validated the experiments, and reviewed and edited the manuscript. C.C., A.M. and R.M. performed the experiments and contributed to data collection and analysis. S.G., S.GH., D.N., A.A., G.A., F.F., V.L. and P.D.B. contributed to writing and revising the manuscript, with P.D.B. also contributing to data supervision. R.MO. performed the statistical analyses. All authors discussed the results and critically commented on the manuscript.

Funding This work was supported by: i) the Italian Ministry of University and Research (the European Union—Next-Generation EU through the Italian Ministry of University and Research under PRIN 2022S74XWB, Missione 4 Componente 2 CUP I53D23005240006 (R.M.); ii) the Italian Ministry of University and Research (the European Union—Next-Generation EU through the Italian Ministry of University and Research under PNRR—M4C2-I1.3 Project PE_00000019 "HEAL ITALIA", CUP I53C22001440006) (R.M.); iii) Alessandra Marzoppi is supported by National Institute for Cardiovascular Research (INRC).

Data Availability Data are available upon request.

Declarations

Declaration of interests Nothing to declare.

References

1. Kurmani S, Squire I. Acute heart failure: definition, classification and epidemiology. Curr Heart Fail Rep. 2017;14:385–92. https://doi.org/10.1007/s11897-017-0351-y.
2. Bozkurt B, Coats AJS, Tsutsui H, Abdelhamid CM, Adamopoulos S, Albert N, et al. Universal definition and classification of heart failure: a report of the Heart Failure Society of America, Heart Failure Association of the European Society of Cardiology, Japanese Heart Failure Society and Writing Committee of the Universal Definition of Heart Failure. Eur J Heart Fail. 2021;23:352–80. https://doi.org/10.1002/ejhf.2115.
3. Edelmann F, Holzendorf V, Wachter R, Nolte K, Schmidt AG, Kraigher-Krainer E, et al. Galectin-3 in patients with heart failure with preserved ejection fraction: results from the Aldo-DHF Trial. Eur J Heart Fail. 2015;17:214–23. https://doi.org/10.1002/ejhf.203.
4. Borlaug BA, Paulus WJ. Heart failure with preserved ejection fraction: pathophysiology, diagnosis, and treatment. Eur Heart J. 2011;32:670–9. https://doi.org/10.1093/eurheartj/ehq426.
5. Fayyaz AU, Eltony M, Prokop LJ, Koepp KE, Borlaug BA, Dasari S, et al. Pathophysiological insights into HFpEF from studies of human cardiac tissue. Nat Rev Cardiol. 2025;22:90–104. https://doi.org/10.1038/s41569-024-01067-1.
6. Tschöpe C, Van Linthout S. New insights in (inter)cellular mechanisms by heart failure with preserved ejection fraction. Curr Heart Fail Rep. 2014;11:436–44. https://doi.org/10.1007/s11897-014-0219-3.
7. Brutsaert DL. Cardiac endothelial-myocardial signaling: its role in cardiac growth, contractile performance, and rhythmicity. Physiol Rev. 2003;83:59–115. https://doi.org/10.1152/physrev.00017.2002.
8. Khan BV, Harrison DG, Olbrych MT, Alexander RW, Medford RM. Nitric oxide regulates vascular cell adhesion molecule 1 gene expression and redox-sensitive transcriptional events in human vascular endothelial cells. Proc Natl Acad Sci U S A. 1996;93:9114–9. https://doi.org/10.1073/pnas.93.17.9114.
9. Wang P, Konja D, Singh S, Zhang B, Wang Y. Endothelial senescence: from macro- to micro-vasculature and its implications on cardiovascular health. Int J Mol Sci. 2024;25(4):1978. https://doi.org/10.3390/ijms25041978.
10. Balistreri CR, Madonna R, Ferdinandy P. Is it the time of seno-therapeutics application in cardiovascular pathological conditions related to ageing? Curr Res Pharmacol Drug Discov. 2021;2:100027. https://doi.org/10.1016/j.crphar.2021.100027.
11. Madonna R, Novo G, Balistreri CR. Cellular and molecular basis of the imbalance between vascular damage and repair in ageing and age-related diseases: as biomarkers and targets for new treatments. Mech Ageing Dev. 2016;159:22–30. https://doi.org/10.1016/j.mad.2016.03.005.
12. Giesen J, Menges L, Benndorf RA. Tissue-specific regulation of NO-GC isoforms in the cardiovascular system. Biochem Pharmacol. 2025;242:117384. https://doi.org/10.1016/j.bcp.2025.117384.
13. Venkatesan S, Smirne C, Aquino CI, Surico D, Remorgida V, Ola Pour MM, et al. Nitric Oxide signaling in cardiovascular physiology and pathology: mechanisms, dysregulation, and therapeutic frontiers. Int J Mol Sci. 2026. https://doi.org/10.3390/ijms27020629.
14. Dushpanova A, Agostini S, Ciofini E, Cabiati M, Casieri V, Matteucci M, et al. Gene silencing of endothelial von Willebrand Factor attenuates angiotensin II-induced endothelin-1 expression in porcine aortic endothelial cells. Sci Rep. 2016;6:30048. https://doi.org/10.1038/srep30048.
15. Pellegrino R, Perpetuini D, Paganelli R, Di Iorio A, Filoni S, Tinari N, et al. Galectin-3-binding protein is a risk factor for diabetes, metabolic syndrome, and inflammation. Cross-sectional and longitudinal results from the InCHIANTI study. Mech Ageing Dev. 2025;226:112086. https://doi.org/10.1016/j.mad.2025.112086.
16. de Boer RA, Edelmann F, Cohen-Solal A, Mamas MA, Maisel A, Pieske B. Galectin-3 in heart failure with preserved ejection fraction. Eur J Heart Fail. 2013;15:1095–101. https://doi.org/10.1093/eurjhf/hft077.
17. Ni CW, Kumar S, Ankeny CJ, Jo H. Development of immortalized mouse aortic endothelial cell lines. Vasc Cell. 2014;6(1):7. https://doi.org/10.1186/2045-824X-6-7.
18. McDonagh TA, Metra M, Adamo M, Gardner RS, Baumbach A, Böhm M, et al. 2021 ESC guidelines for the diagnosis and treatment of acute and chronic heart failure. Eur Heart J. 2021;42:3599–726. https://doi.org/10.1093/eurheartj/ehab368.
19. Reddy YNV, Carter RE, Obokata M, Redfield MM, Borlaug BA. A simple, evidence-based approach to help guide diagnosis of heart failure with preserved ejection fraction. Circulation. 2018;138:861–70. https://doi.org/10.1161/CIRCULATIONAHA.118.034646.
20. Hughes CS, Moggridge S, Müller T, Sorensen PH, Morin GB, Krijgsveld J. Single-pot, solid-phase-enhanced sample preparation for proteomics experiments. Nat Protoc. 2019;14(1):68–85. https://doi.org/10.1038/s41596-018-0082-x.
21. Potenza F, Cufaro MC, Di Biase L, Panella V, Di Campli A, Ruggieri AG, Dufrusine B, Restelli E, Pietrangelo L, Protasi F, Pieragostino D, De Laurenzi V, Federici L, Chiesa R, Sallese M. Proteomic Analysis of Marinesco-Sjogren Syndrome Fibroblasts Indicates Pro-Survival Metabolic Adaptation to SIL1 Loss. Int J Mol Sci. 2021;22(22):12449. https://doi.org/10.3390/ijms222212449.
22. Madonna R, Moscato S, Polizzi E, Pieragostino D, Cufaro MC, Del Boccio P, et al. Connexin 43 and Connexin 26 Involvement in the Ponatinib-Induced Cardiomyopathy: Sex-Related Differences in a Murine Model. Int J Mol Sci. 2021;22(11):5815. https://doi.org/10.3390/ijms22115815.
23. Cox J, Hein MY, Luber CA, Paron I, Nagaraj N, Mann M. Accurate proteome-wide label-free quantification by delayed normalization and maximal peptide ratio

extraction, termed MaxLFQ. Mol Cell Proteomics. 2014;13(9):2513–26. https://doi.org/10.1074/mcp.M113.031591.
24. Krämer A, Green J, Pollard J Jr, Tugendreich S. Causal analysis approaches in ingenuity pathway analysis. Bioinformatics. 2014;30(4):523–30. https://doi.org/10.1093/bioinformatics/btt703.
25. Esposito C, Fasoli G, Plati AR, Bellotti N, Conte MM, Cornacchia F, et al. Long-term exposure to high glucose up-regulates VCAM-induced endothelial cell adhesiveness to PBMC. Kidney Int. 2001;59(5):1842–9. https://doi.org/10.1046/j.1523-1755.2001.0590051842.x.
26. Madonna R, De Caterina R. Prolonged exposure to high insulin impairs the endothelial PI3-kinase/Akt/nitric oxide signalling. Thromb Haemost. 2009;101(2):345–50.
27. Renström F, Burén J, Svensson M, Eriksson JW. Insulin resistance induced by high glucose and high insulin precedes insulin receptor substrate 1 protein depletion in human adipocytes. Metabolism. 2007;56(2):190–8. https://doi.org/10.1016/j.metabol.2006.09.012.
28. Cabiati M, Biondi F, Ghelardoni S, Casieri V, Lionetti V, Sgalippa A, et al. Ambrisentan retains its pro-autophagic activity on human pulmonary artery endothelial cells exposed to hypoxia in an in vitro model mimicking diabetes. J Cell Mol Med. 2025;29(7):e70528. https://doi.org/10.1111/jcmm.70528.
29. Ungvari Z, Podlutsky A, Sosnowska D, Tucsek Z, Toth P, Deak F, et al. Ionizing radiation promotes the acquisition of a senescence-associated secretory phenotype and impairs angiogenic capacity in cerebromicrovascular endothelial cells: role of increased DNA damage and decreased DNA repair capacity in microvascular radiosensitivity. J Gerontol A Biol Sci Med Sci. 2013;68(12):1443–57. https://doi.org/10.1093/gerona/glt057.
30. Zhong C, Li P, Argade S, Liu L, Chilla' A, Liang W, et al. Inhibition of protein glycosylation is a novel pro-angiogenic strategy that acts via activation of stress pathways. Nat Commun. 2020;11(1):6330. https://doi.org/10.1038/s41467-020-20108-0. (**Erratum in: Nat Commun. 2025 Dec 8;16(1):10936. doi: 10.1038/s41467-025-67407-y**).
31. AbouEzzeddine OF, Haines P, Stevens S, Nativi-Nicolau J, Felker GM, Borlaug BA, et al. Galectin-3 in heart failure with preserved ejection fraction. JACC Heart Fail. 2015;3(3):245–52. https://doi.org/10.1016/j.jchf.2014.10.009.
32. Huang J, Chen J, Xu S, Zhang H, Ni M, Wang A, et al. Effects of dapagliflozin on ventricular remodeling and prognosis in older females with heart failure with preserved ejection fraction: A single-center prospective study. Exp Gerontol. 2025;211:112926. https://doi.org/10.1016/j.exger.2025.112926.
33. Piccolo E, Tinari N, Semeraro D, Traini S, Fichera I, Cumashi A, et al. LGALS3BP, lectin galactoside-binding soluble 3 binding protein, induces vascular endothelial growth factor in human breast cancer cells and promotes angiogenesis. J Mol Med. 2013;91:83–94. https://doi.org/10.1007/s00109-012-0936-6.
34. Barman SA, Li X, Haigh S, Kondrikov D, Mahboubi K, Bordan Z, et al. Galectin-3 is expressed in vascular smooth muscle cells and promotes pulmonary hypertension through changes in proliferation, apoptosis, and fibrosis, American Journal of Physiology-Lung Cellular and Molecular. Physiology. 2019;316:L784–97. https://doi.org/10.1152/ajplung.00186.2018.
35. Budde H, Hassoun R, Mügge A, Kovács Á, Hamdani N. Current understanding of molecular pathophysiology of heart failure with preserved ejection fraction. Front Physiol. 2022. https://doi.org/10.3389/fphys.2022.928232.
36. Xia N, Förstermann U, Li H, Implication of eNOS Uncoupling in Cardiovascular Disease, Reactive Oxygen Species. 2017. https://doi.org/10.20455/ros.2017.807.
37. Carresi C, Mollace R, Macrì R, Scicchitano M, Bosco F, Scarano F, et al. Oxidative stress triggers defective autophagy in endothelial cells: role in atherothrombosis development. Antioxidants. 2021;10:387. https://doi.org/10.3390/antiox10030387.
38. Janaszak-Jasiecka A, Płoska A, Wierońska JM, Dobrucki LW, Kalinowski L. Endothelial dysfunction due to eNOS uncoupling: molecular mechanisms as potential therapeutic targets. Cell Mol Biol Lett. 2023;28:21. https://doi.org/10.1186/s11658-023-00423-2.
39. Milan M, Troyano-Rodriguez E, Ihuoma J, Negri S, Rudraboina R, Kosmider A, et al. Fasting as medicine: Mitochondrial and endothelial rejuvenation in vascular aging. Aging Cell. 2026;25(2):e70372. https://doi.org/10.1111/acel.70372.
40. Zhao S, Zhao C, Wang L, Cheng B, Zheng M, Wang X. Elucidating the role of LGALS3BP in coronary atherosclerosis: integrating bioinformatics and machine learning for advanced insights. J Cardiothorac Surg. 2025;20:338. https://doi.org/10.1186/s13019-025-03462-2.

Publisher's Note Springer Nature remains neutral with regard to jurisdictional claims in published maps and institutional affiliations.

Springer Nature or its licensor (e.g. a society or other partner) holds exclusive rights to this article under a publishing agreement with the author(s) or other rightsholder(s); author self-archiving of the accepted manuscript version of this article is solely governed by the terms of such publishing agreement and applicable law.